ACS APPLIED MATERIALS & INTERFACES

Research Article

www.acsami.org

Fabricate Heterojunction Diode by Using the Modified Spray Pyrolysis Method to Deposit Nickel–Lithium Oxide on Indium Tin Oxide Substrate

Chia-Ching Wu[†] and Cheng-Fu Yang*[,‡]

[†]Department of Electronic Engineering, Kao Yuan University, Kaohsiung, Taiwan, R.O.C.

[‡]Department of Chemical and Materials Engineering, National University of Kaohsiung, Kaohsiung, Taiwan, R.O.C.

ABSTRACT: P-type lithium-doped nickel oxide (p-LNiO) thin films were deposited on an n-type indium tin oxide (ITO) glass substrate using the modified spray pyrolysis method (SPM), to fabricate a transparent p–n heterojunction diode. The structural, optical, and electrical properties of the p-LNiO and ITO thin films and the p-LNiO/n-ITO heterojunction diode were characterized by field emission scanning electron microscopy (FE-SEM), X-ray diffraction (XRD), UV–visible spectroscopy, Hall effect measurement, and current–voltage (I–V) measurements. The nonlinear and rectifying I–V properties confirmed that a heterojunction diode characteristic was successfully formed in the p-LNiO/n-ITO (p–n) structure. The I–V characteristic was dominated by space-charge-limited current (SCLC), and the Anderson model demonstrated that band alignment existed in the p-LNiO/n-ITO heterojunction diode.

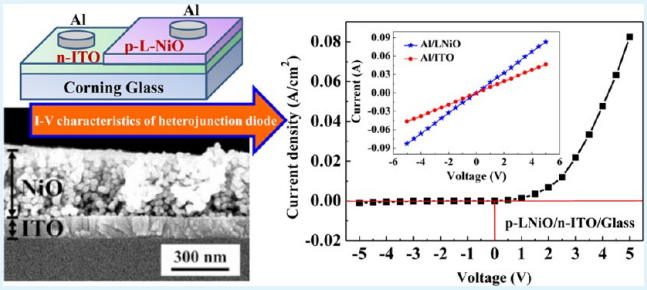

KEYWORDS: *heterojunction, nickel–lithium oxide, modified spray pyrolysis method, current–voltage characteristic*

INTRODUCTION

"Transparent electronics" is an emerging technology that employs wide band gap semiconductors to realize invisible circuits for next-generation optoelectronic devices.[1−3] Transparent conducting oxide (TCO) materials, which exhibit high optical transparency and electrical conductivity and can be grown efficiently as thin films, are used extensively for a variety of applications, including transparent electronic devices. Most of the well-known and widely used TCO thin films, such as zinc oxide (ZnO), tin oxide (SnO_2), indium tin oxide (ITO), and so forth, are n-type materials. Surprisingly, their corresponding p-type transparent conducting oxides were for a long time not a focus of interest. In recent years, numerous reports have been published on p-type transparent conducting oxides, such as $CuAlO_2$, $LaCuO_2$, and $SrCu_2O_2$.[4−6] Nickel oxide (NiO) thin films are promising p-type semi-TCO candidates for visible light, and NiO is a suitable material for fabricating a p-n heterojunction diode. Recently, ZnO/NiO and MgZnO/NiO heterojunctions have been fabricated using various thin film preparation technologies.[7,8]

The conduction properties of NiO thin films are primarily determined by holes generated from nickel vacancies, oxygen interstitial atoms, and the use of a dopant. The resistivity of NiO thin films can be decreased by doping with monovalent impurities, such as lithium (Li).[9,10] According to the literature, NiO thin films have been prepared by sputtering,[11] chemical vapor deposition (CVD),[12] and the spray pyrolysis method (SPM).[13] SPM is a very important technique for fabricating TCO thin films because it is a relatively simple atmospheric pressure deposition method and is inexpensive for large-area coating. However, doped NiO thin films prepared by SPM have larger resistivity than those deposited by other methods. The traditional SPM involves spraying nickel nitrate solution onto a preheated glass substrate (>300 °C), which then undergoes evaporation, solute precipitation, and pyrolytic decomposition. As the substrate temperature is increased, the evaporation ratio of the solution on the substrate is too swift, resulting in the formation of inferior NiO thin films.

In the present research, a modified SPM was used to develop p-LNiO thin films with higher conductivity. We investigated the effects of Li concentration on the electrical, optical, and physical properties of the p-LNiO thin films. The p–n heterojunction diodes were fabricated by using a modified SPM to deposit Li-doped p-type NiO (p-LNiO) thin films on an ITO glass substrate. The I–V characteristics confirmed that the p-LNiO/n-ITO heterojunction had diode properties. The space-charge-limited current (SCLC) and the Anderson model demonstrated the current transport and band alignment mechanism of the p-LNiO/n-ITO heterojunction diode.

Received: February 28, 2013
Accepted: May 17, 2013
Published: May 17, 2013

EXPERIMENTAL SECTION

P-type lithium-doped nickel oxide (p-LNiO) thin films were deposited on the n-ITO glass substrate (UR-ITO007−0.7 mm, 7 Ω/per square, Unionward Corp., Taipei, Taiwan) using a modified SPM. Figure 1

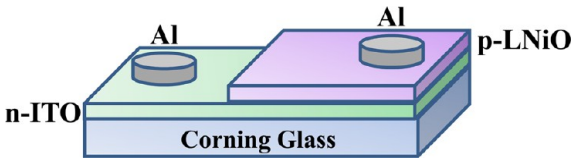

Figure 1. Schematic diagram of the p-LNiO/n-ITO heterojunction structure.

shows the schematic structure of the p-LNiO/n-ITO heterojunction diode on the glass substrate. Thin films of p-LNiO were prepared using a solution of lithium nitrate ($LiNO_3$, J.T. Barker, U.S.A.) and nickel nitrate ($Ni(NO_3)_2{\cdot}6H_2O$, Alfa Aesar, U.S.A.) in deionized water. The concentration of Li in the p-LNiO thin films increased from 2 to 8 at%. The p-LNiO thin films were baked at 140 °C and crystallized at 600 °C. Aluminum (Al) electrodes were deposited using electron beam evaporation, and the area of the Al was 0.0078 cm^2. The crystalline structures of the p-LNiO thin films were determined with an X-ray diffractometer (XRD) using CuKα radiation (K = 1.5418 Å). The atomic bonding states of the p-LNiO thin films were analyzed using X-ray photoemission spectroscopy (XPS). To determine the transmittance of the thin films, an optical transmission study was carried out in the wavelength range 200−1100 nm, using a Hitachi 330 spectrophotometer. The electrical resistivity and the Hall-effect coefficients were measured using a Bio-Rad Hall setup. The cross sections and surface morphologies of the p-LNiO thin films and p-LNiO/n-ITO heterojunction diodes were examined with a field emission scanning electron microscope (FE-SEM). The current−voltage (I−V) characteristics of the p-LNiO/n-ITO heterojunction diodes were measured with an HP4156 semiconductor parameter analyzer. The measurements were performed by changing the bias voltages from +5 to −5 V.

3. RESULTS AND DISCUSSION

The cross-section and surface SEM images in Figure 2 confirm that the p-LNiO thin films had a polycrystalline structure and their thicknesses were about 350 nm for all Li concentrations. From the surface SEM images (inset Figure 2) and the results calculated from the Scherrer formula (Figure 5) we can determine that the aggregate particle sizes of the p-LNiO thin films increased from 18 to 52 nm as the Li concentration increased from 2 to 8 at %. At Li = 2 at % and Li = 4 at %, the surface morphology of the p-LNiO thin film was smooth but not compact. As the Li concentration was increased, particle aggregations in the p-LNiO thin films were observed, as was a decrease in the number of pores in the surface morphology. These results were due to the liquid phase sintering phenomenon, which occurred as Li was added to the p-LNiO thin films.[14] The crystallization of the modified SPM-deposited LNiO thin films was better than that of traditional SPM-deposited LNiO thin films and similar to sputter-deposited thin films. Figure 3 shows a cross-section SEM image of a p-LNiO thin film deposited on an n-ITO substrate, using the modified SPM to form a p-n heterojunction diode. The thickness of the n-ITO thin film was about 150 nm and the thickness of the modified SPM p-LNiO thin film was approximately 350 nm, as shown in Figure 3.

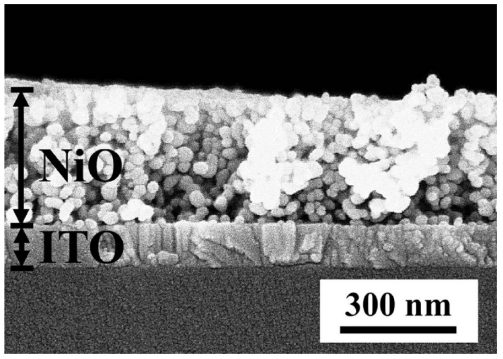

Figure 3. Cross-section SEM image of the p-LNiO/n-ITO heterojunction diode.

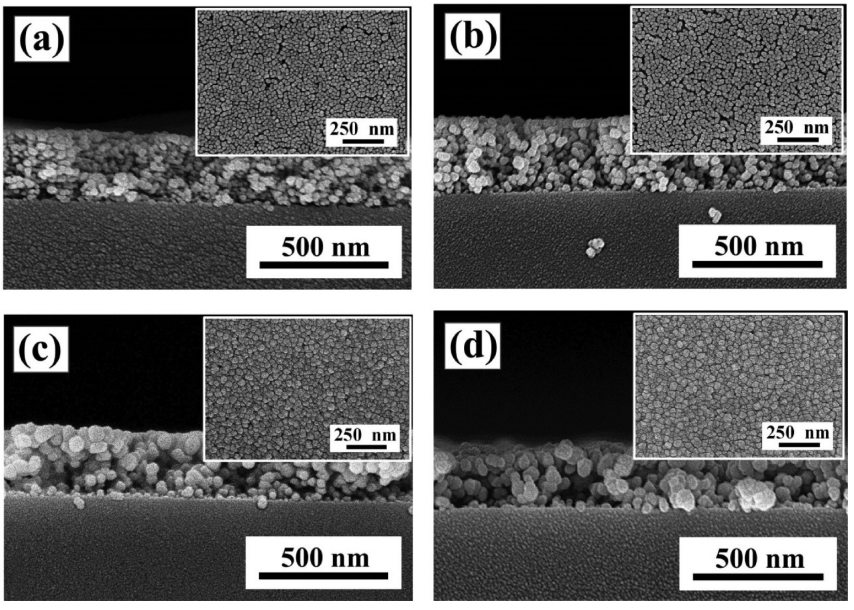

Figure 2. Cross-section and surface SEM images of the p-LNiO thin films as a function of Li concentration: (a) 2, (b) 4, (c) 6, and (d) 8 at %.

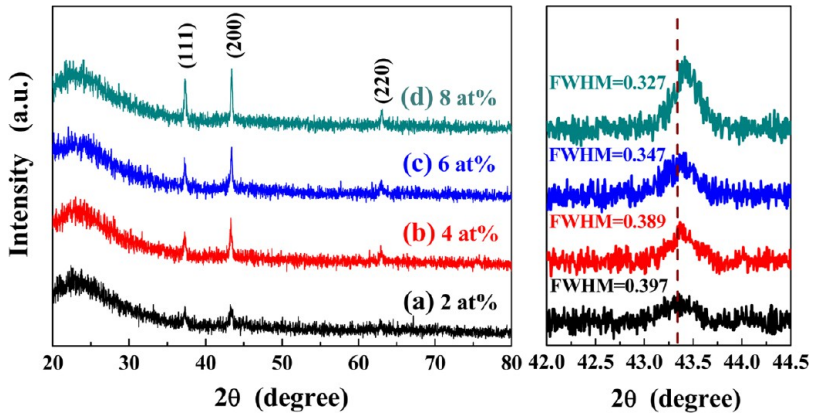

Figure 4. XRD pattern of the p-LNiO thin films as a function of Li concentration.

The XRD patterns of the p-LNiO thin films as a function of Li concentration are shown in Figure 4. The diffraction peaks revealed at 2θ values of 37.3, 43.2, and 63.1° correspond to the (111), (200), and (220) planes of the p-LNiO thin films (cubic unit cell). The diffraction intensities of the (111), (200), and (220) peaks of the p-LNiO thin films increased with Li concentration. These increases are attributed to grain growth, because the full width half-maximum (fwhm) of the (200) diffraction peak decreased as the Li concentration increased, as shown in Figure 5. The 2θ value for the (200) diffraction peak

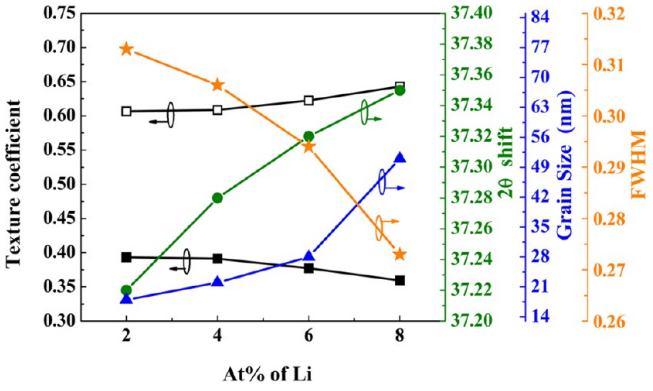

Figure 5. Texture coefficient (solid square line: (111) phase; open square line: (200) phase), 2θ shift (solid circle line), grain sizes (solid triangle line), and fwhm (solid star line) of the p-LNiO thin films as a function of Li concentration.

of the p-LNiO thin films shifted from 43.26 to 43.43° as the Li concentration increased from 2 to 8 at %, also shown in Figure 5. This implies that the smaller radius of Li^+ ions (0.6 Å) allows them to substitute in the positions of the larger Ni^{2+} ions (0.69 Å), which decreases the lattice constant of the p-LNiO thin films. A previous report indicated that Li ions occupy the interstitial sites and increase the lattice constant in the Ni−Li−O system.[15] On the basis of our results, the doped mechanism for the variation of lattice constant demonstrated that Li ions replace the sites of Ni ions in the p-LNiO thin films. We use the following texture coefficient (TC) equation[16]

$$TC_{(hkl)} = \frac{I_{(hkl)}}{\sum I_{(hkl)}} \times 100 \quad (1)$$

where h, k, and l are the Miller indices, $TC_{(hkl)}$ is the TC value of the specific (hkl) plane, $I_{(hkl)}$ is the measured peak intensity, and $\Sigma I_{(hkl)}$ is the summation of all intensities for the peaks of p-LNiO thin films. As the Li concentration increased from 2 to 8 at %, the $TC_{(111)}$ value decreased from 0.394 to 0.357, and the $TC_{(200)}$ value changed from 0.602 to 0.641. The (200) plane of ionic rock salt materials is considered a nonpolar cleavage plane and is thermodynamically stable; it is the most stable NiO termination with a surface energy. Therefore, the (200) preferred orientation of p-LNiO thin films can result in better conductive properties and resistance to electrical aging.

The Ni $2p_{3/2}$ and O 1s XPS spectra of the p-LNiO thin films is shown in panels a and b in Figure 6 as a function of Li concentration. In all the LNiO thin films, the Ni $2p_{3/2}$ electron the deconvolution of binding energy for the NiO peak (Ni^2+)

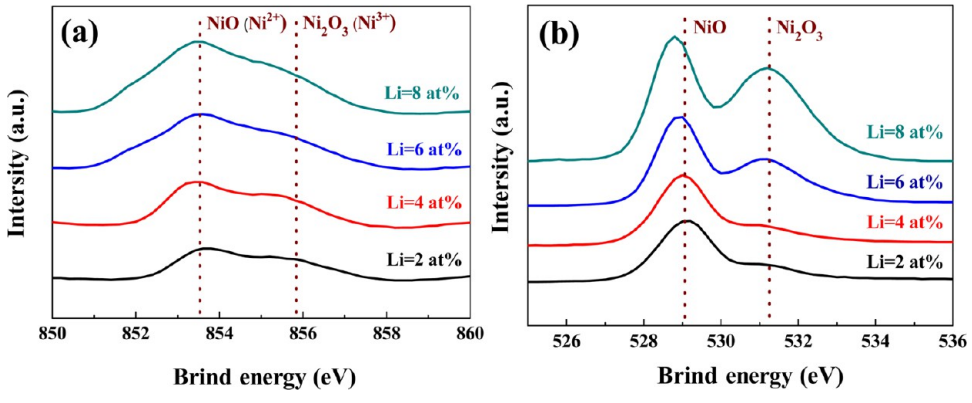

Figure 6. XPS spectra of (a) Ni $2p_{3/2}$ and (b) O 1s core levels of the p-LNiO thin films as a function of Li concentration.

at 854.0 eV and the Ni_2O3 (Ni^3+) peak at 855.8 eV was observed.[17,18] There was no significant difference, such as a peak shift in the $Ni_2p_{3/2}$ spectrum, as a function of Li concentration. The intensities of the Ni^{2+} and Ni^{3+} bonding states increased, and the Ni^{2+} bonding state increased slightly over the Ni^{3+} bonding state, as Li concentration increased in the p-LNiO thin films. This was also confirmed by the O 1s XPS spectrum, as shown in Figure 6b. Deconvolution of the electron binding energy of the NiO (529.3 eV) and Ni_2O_3 (531.9 eV) occurred in the p-LNiO thin films,[17−21] and the intensity of the O 1s peak increased as Li concentration increased.

Several groups have demonstrated that the formation of holes in a NiO thin film was due to an increase in the Ni^{3+} ions or to the formation of Ni^{2+} vacancies and the presence of interstitial oxygen atoms.[22,23] Many Ni^{2+} vacancies exist in a nonstoichiometric NiO thin film, and some Ni^{2+} ions are oxidized to Ni^{3+} ions to keep the charge near the Ni^{2+} vacancies natural.[24] Table 1 lists the Li, Ni, and O atomic percentages,

Table 1. Li, Ni, and O Ratios of the p-LNiO Thin Films, Measured by XPS

	Ni (at %)	O (at %)	Li (at %)	O/Ni
2 at %	44.7	53.5	1.8	1.1968
4 at %	43.2	52.9	3.9	1.2245
6 at %	41.1	52.7	6.2	1.2822
8 at %	39.4	52.5	8.1	1.3325

determined by XPS analysis, and the O/Ni ratios. The O/Ni ratios of the p-LNiO thin films increased with Li concentration from 1.1968 to 1.3325. This means that the excess oxygen in the p-LNiO thin films created Ni^{2+} vacancies, which subsequently were ionized, forming Ni^{3+} ions and holes.[25] With the increase in hole concentration of the p-LNiO thin films, the carrier concentration increased, as did the conductivity.

Table 2 shows the electrical properties of the p-LNiO thin films as a function of Li concentration, the all samples reveal

Table 2. Resistivity, Mobility, And Carrier Concentration of the p-LNiO Thin Films As a Function of Li Concentration

Li	concentration (cm^{-3})	mobility ($cm^2/(V\ s)$)	resistivity (Ω cm)	type (N/P)
2 at %	1.91×10^{17}	11.96	1.98	p-type
4 at %	3.83×10^{17}	8.53	1.32	p-type
6 at %	9.37×10^{17}	3.56	0.91	p-type
8 at %	1.19×10^{18}	2.26	0.41	p-type

that the p-type properties. The resistivity of 2 at% Li-doped NiO thin film was 1.98 Ω-cm, increasing with Li concentration to a maximum value of 4.1×10^{-1} Ω-cm at 8 at%. This occurred because as the Li concentration increased from 2 to 8 at%, the numbers of Li atoms to replace the sites of Ni atoms increased, and the carrier (hole) concentration increased from 1.91×10^{17} to 1.19×10^{18} cm^{-3}. The carrier mobility of the p-LNiO thin films decreased from 11.96 to 2.26 $cm^2/(V\ s)$ as the Li concentration increased from 2 to 8 at %. In p-LNiO thin films, dopant materials can act as scattering centers; as the Li concentration increases, the carrier encounters more hindering materials, with a resultant decrease in carrier mobility.

Figure 7a shows the transmittance spectra of p-L8NiO (Li = 8 at%) and n-ITO thin films, and of p-L8NiO/n-ITO heterojunction diodes, respectively. The p-L8NiO and n-ITO thin films show a high transmittance in the range of visible light and a sharp absorption edge at 400 nm, indicating that they can be used as transparent windows. Transmittance of more than 70% at a typical wavelength of 600 nm was observed across the p-L8NiO/n-ITO heterojunction diodes. This value is similar to what was reported for an ITO/CdO transparent heterojunction diode and a p-$CuAlO_2$/n-ZnO:Al transparent heterojunction diode fabricated using the vacuum system.[26,27] The optical energy bandgap (E_g) values of those thin films were calculated using transmittance data. According to the transmission spectra, the E_g of the p-L8NiO and n-ITO thin films and p-L8NiO/n-ITO heterojunction diodes can be determined. The method is based on the following relation[28]

$$\alpha h\nu = A(h\nu - E_g)^n \quad (2)$$

where α is the absorption coefficient, $h\nu$ is the photon energy, A is a constant, E_g is the optical energy bandgap (eV), and n is the type of energy bandgap. Figure 7b presents the plots of $(\alpha h\nu)^{1/2}$ versus hν (photon energy) for the p-L8NiO and n-ITO thin films and the p-L8NiO/n-ITO heterojunction diodes. The E_g values of those thin films have been obtained by extrapolating from the linear portion of the graph.[29] As shown in Figure 7b, the E_g values of the p-L8NiO and n-ITO thin films are 2.89 and 3.32 eV, respectively. The E_g value of the p-L8NiO/n-ITO heterojunction diode was 2.73 eV. As eq 2 shows, the E_g value can be influenced by the transparent curve of the bilayer p-L8NiO/n-ITO heterojunction structure. This is because the interface between the p-L8NiO and n-ITO layers may not be uniform, and there is a possibility of interface mixing, impurity, and/or substrate diffusion during the annealing possess. Furthermore, the decreased optical transparency across the junction also indicates that light scattering centers exist at the oxide interface and that the E_g value decreases.[30]

The nonlinear and rectifying $I-V$ characteristics of the heterojunction diodes confirm that a p-n junction structure was successfully formed in all bilayer p-LNiO/n-ITO structures. When 8 at % Li was added to the NiO thin films, the p-L8NiO/n-ITO heterojunction diodes had lower turn-on voltages and higher rectification ratios. Figure 8a shows the current−voltage ($I-V$) characteristics of the p-L8NiO and n-ITO thin films and the p-L8NiO/n-ITO heterojunction diodes. The Al can be used as the electrodes of transparent p-NiO/n-ZnO heterojunction devices for ultraviolet photodetectors because of its ohmic-contact behavior.[31] This ohmic-contact behavior is confirmed by the fairly linear $I-V$ characteristics of the Al/p-LNiO and Al/n-ITO thin films, as shown in the inset for Figure 8a. Under forward bias, the lower value of the turn-on voltage of the p-L8NiO/n-ITO heterojunction diode is about 0.8 V, which is similar to values in other reports using the vacuum deposition method of fabrication.[32] In this study, the leakage current is 4.99×10^{-6} A/cm^2 at 2 V for the p-L8NiO/n-ITO heterojunction diodes, as shown in Figure 8b, slightly larger than in other reports. The higher leakage current results from defects or imperfections between the heterojunction interfaces of the p-L8NiO and n-ITO thin films.

The log ($|I|$)−log(V) curve is plotted in Figure 9. As the forward voltage is lower than 0.3 V, the I value is linearly dependent on V^1, indicating that the transport mechanism obeys Ohm's law. As the forward voltage is higher than 1.3 V, the I value is dependent on V^2, which is dominated by the space-charge-limited current (SCLC) mechanism.[33,34] Non-

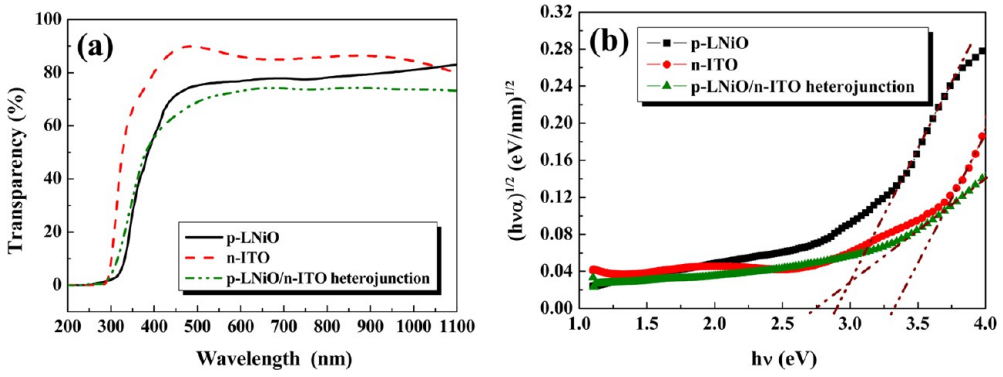

Figure 7. (a) UV−vis spectra and (b) $(\alpha h\nu)^2$ vs $h\nu$ plots of the p-L8NiO and n-ITO thin films and p-L8NiO/n-ITO heterojunction diodes.

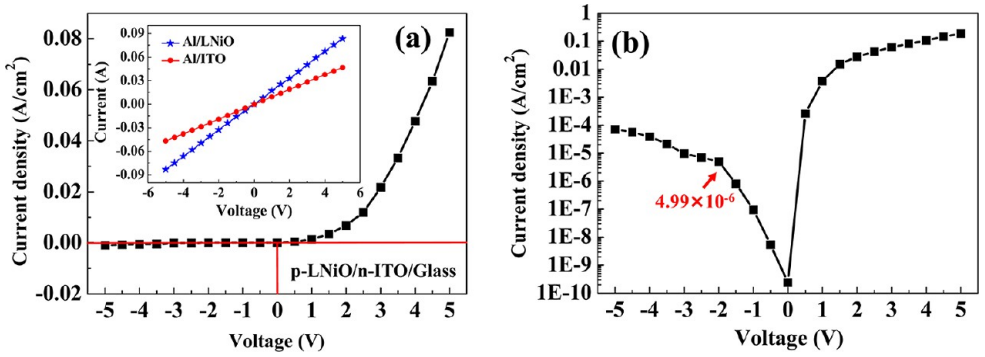

Figure 8. (a) $I-V$ characteristics and (b) log (|I|)−log(V) curve of the p-L8NiO/n-ITO heterojunction diodes.

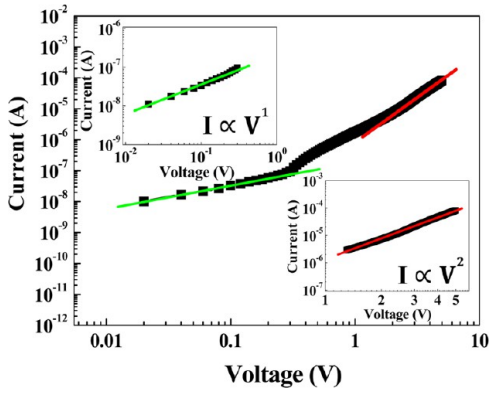

Figure 9. Log (|I|)−log(V) curve of the p-L8NiO/n-ITO heterojunction diodes.

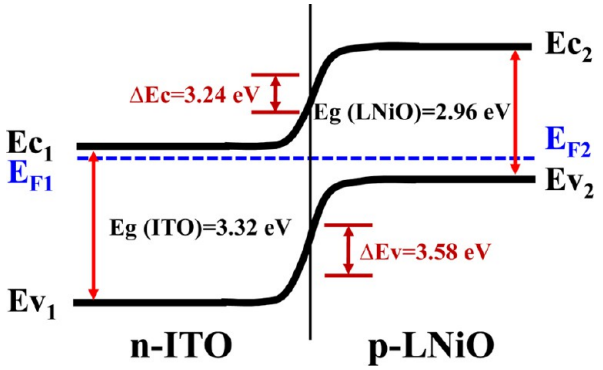

Figure 10. Energy-band diagram of the p-L8NiO/n-ITO heterojunction diodes under zero bias.

ohmic behavior has often been interpreted in terms of a trap-controlled SCLC. In the intermediate region, 0.4 V < V < 1.1 V, this transition region often appears with the presence of traps near the Fermi level of the layer in which the SCLC flow occurs. The SCLC phenomenon is caused by nonideal situations, including oxide vacancy, grain boundary, dopant, and defects in the p-LNiO thin films. The ideal SCLC mechanism is observed in a perfect insulator that is free of traps. In practice, our p-L8NiO/n-ITO heterojunction diodes are not ideal.

Figure 10 shows an idealized energy band diagram of the p-L8NiO/n-ITO heterojunction diodes, as deduced from the Anderson model.[31] The electron affinity ($q\chi$) of the p-L8NiO thin films was measured with cyclic voltammetry, yielding a value of about 1.46 eV.[35] The $q\chi$ value of the n-ITO thin films was 4.7 eV,[36] and the energy band gaps (E_g) were 2.98 and 3.32 eV for the p-L8NiO and n-ITO thin films, respectively. We therefore can determine the differences in conduction band offset (CBO) voltage and valence band offset (VBO) voltage between the heterojunction materials. According to the Anderson model, the energy barrier to electrons is

$$\mathrm{CBO} = \Delta E_c = q(\chi_{\mathrm{ITO}} - \chi_{\mathrm{LNiO}}) = 4.7 - 1.46 = 3.24 \text{ eV}$$

$$\begin{aligned}\mathrm{VBO} &= \Delta E_v \\ &= E_{g(\mathrm{ITO})} + q\chi_{\mathrm{ITO}} - [E_{g(\mathrm{LNiO})} + \chi_{\mathrm{LNiO}}] \\ &= E_{g(\mathrm{ITO})} - E_{g(\mathrm{LNiO})} + \Delta E_c \\ &= 3.32 - 2.98 + 3.24 \\ &= 3.58 \text{ eV}\end{aligned}$$

dx.doi.org/10.1021/am400763m | ACS Appl. Mater. Interfaces 2013, 5, 4996−5001

The conduction band level of the p-L8NiO thin films is higher than that of n-ITO, which means that a type II alignment forms at the interface of the p-L8NiO/n-ITO heterojunction. In addition, the ratio of CBO to VBO is estimated to be about 0.91. This result demonstrates that the electrons easily transition to the energy barrier, whereupon a lower turn-on voltage is obtained with the p-L8NiO/n-ITO heterojunction diode (V = 0.8 V).

CONCLUSIONS

Transparent p−n heterojunction diodes consisting of bilayer p-L8NiO and n-ITO thin films were successfully fabricated and characterized. Nonvacuum SPM was used to deposit high-quality p-LNiO thin films. The p-L8NiO/n-ITO heterojunction diodes had an average transmittance of over 70% in the visible region. The current−voltage (I−V) showed that the lower turn-on voltage was about 0.8 V and the leakage current was 1.94×10^{-4} A/cm^2 at 1 V for the p-L8NiO/n-ITO heterojunction diodes. The log ($|I|$) − log(V) curve indicated that the space-charge-limited current dominated the current transport. A type-II band alignment of p-L8NiO/n-ITO heterojunction diode with a valence band offset voltage of E_V = 3.58 eV and a conduction band offset voltage of E_C = 3.24 eV were obtained.

AUTHOR INFORMATION

Corresponding Author

*E-mail: cfyang@nuk.edu.tw.

Notes

The authors declare no competing financial interest.

ACKNOWLEDGMENTS

The authors acknowledge the NSC for 101-2221-E-244-006 and 101-3113-S-244-001.

REFERENCES

(1) Hosono, H. *Thin Solid Films* **2007**, *515*, 6000−6014.
(2) Fortunato, E.; Barquinha, P.; Pimentel, A.; Gonçalves, A.; Marques, A.; Pereira, L.; Martins, R. *Adv. Mater.* **2005**, *17*, 590−594.
(3) Wager, J. F. *Science* **2003**, *300*, 1245−1246.
(4) Gong, H.; Wang, Y.; Luo, Y. *Appl. Phys. Lett.* **2000**, *76*, 3959−3961.
(5) Hidenori, H.; Masahiro, O.; Hirano, M.; Ueda, K.; Hosono, H. *J. Appl. Phys.* **2002**, *91*, 9177−9181.
(6) Ohta, H.; Orita, M.; Hirano, M.; Yagi, I.; Ueda, K.; Hosono, H. *J. Appl. Phys.* **2002**, *91*, 3074−3078.
(7) Vygranenko, Y.; Wang, K.; Nathan, A. *Appl. Phys. Lett.* **2006**, *89*, 172105−172107.
(8) Chen, X.; Ruan, K.; Wu, G.; Bao, D. *Appl. Phys. Lett.* **2008**, *93*, 112112−112114.
(9) Joseph, D. P.; Saravanan, M.; Muthuraaman, B.; Renugambal, P.; Sambasivam, S.; Raja, S. P.; Maruthamuthu, P.; Venkateswaran, C. *Nanotechnology* **2008**, *19*, 485707−485710.
(10) Joshi, U. S.; Matsumoto, Y.; Itaka, K.; Sumiya, M.; Koinuma, H. *Appl. Surf. Sci.* **2006**, *252*, 2524−2528.
(11) Jang, W. L.; Lu, Y. M.; Hwang, W. S.; Hsiung, T. L.; Wang, H. P. *Surf. Coat. Technol.* **2008**, *202*, 5444−5447.
(12) Min, K. C.; Kim, M.; You, Y. H.; Lee, S. S.; Lee, Y. K.; Chung, T. M.; Kim, C. G.; Hwang, J. H.; An, K. S.; Lee, N. S.; Kim, Y. *Surf. Coat. Technol.* **2007**, *201*, 9252−9255.
(13) Reguig, B. A.; Khelil, A.; Cattin, L.; Morsli, M.; Bernède, J. C. *Appl. Surf. Sci.* **2007**, *253*, 4330−4334.
(14) Ham, Y. S.; Koh, J. H. *J. Korean Phys. Soc.* **2009**, *55*, 789−793.
(15) Jarzebski, Z. M. *Oxide Semiconductors*; Pergamon Press: Oxford, U.K., 1973; Vol. *4*, pp 150, 184−186.
(16) Zheng, Z.; Li, N.; Wang, C. Q.; Li, D. Y.; Zhu, Y. M.; Wu, G. *Int. J. Hydrogen Energy* **2012**, *37*, 13921−13932.
(17) Yu, G. H.; Zhu, F. W.; Chai, C. L. *Appl. Phys. A: Mater. Sci. Process.* **2003**, *76*, 45−47.
(18) Oswald, S.; Bruckner, W. *Surf. Interface Anal.* **2004**, *36*, 17−22.
(19) Tanaka, S.; Taniguchi, M.; Tanigawa, H. *J. Nucl. Mater.* **2000**, *283*−*287*, 1405−1408.
(20) Dedryvère, R.; Laruelle, S.; Grugeon, S.; Poizot, P.; Gonbeau, D.; Tarascon, J. M. *Chem. Mater.* **2004**, *16*, 1056−1061.
(21) Wu, Q. H.; Thissen, A.; Jaegermann, W. *Appl. Surf. Sci.* **2005**, *250*, 57−62.
(22) Nandy, S.; Saha, B.; Mitra, M. K. *J. Mater. Sci.* **2007**, *42*, 5766−5772.
(23) Chang, H. L.; Lu, T. C.; Kuo, H. C.; Wang, S. C. *J. Appl. Phys.* **2006**, *100*, 124503−124503−5.
(24) Sasi, B.; Gopchandran, K. G. *Nanotechnology* **2007**, *18*, 115613−115621.
(25) Yun, D. J.; Rhee, S. W. *J. Electrochem. Soc.* **2008**, *155*, H899−H902.
(26) Mohamed, H. A.; Ali, H. M. *Sci. Technol. Adv. Mater.* **2008**, *9*, 025016−025025.
(27) Cheong, W. S.; Yoon, S. M.; Shin, J. H.; Hwang, C. S. *Jpn. J. Appl. Phys.* **2009**, *48*, 04C090−04C094.
(28) Jiang, M.; Liu, X.; Chen, G.; Cheng, J.; Zhou, X. *J. Mater. Sci.* **2009**, *20*, 1225−1228.
(29) Sarkar, A.; Ghosh, S.; Chaudhuri, S.; Pal, A. K. *Thin Solid Films* **1991**, *204*, 255−264.
(30) Mistry, B. V.; Bhatt, P.; Bhavsar, K. H.; Trivedi, S. J.; Trivedi, U. N.; Joshi, U. S. *Thin Solid Films* **2011**, *519*, 3840−3843.
(31) Tsai, S. Y.; Hon, M. H.; Lu, Y. M. *Solid-State Electron.* **2011**, *63*, 37−41.
(32) Pethuraja, G. G; Welser, R. E.; Sood, A. K.; Lee, C.; Alexander, N. J.; Efstathiadis, H.; Haldar, P.; Harvey, J. L. *Adv. Mater. Phys. Chem.* **2012**, *2*, 59−62.
(33) Wang, C. X.; Yang, G. W.; Zhang, T. C.; Liu, H. W.; Han, Y. H.; Luo, J. F.; Gao, C. X.; Zou, G. T. *Diamond Relat. Mater.* **2003**, *12*, 1548−1552.
(34) Yilmaz, K.; Parlak, M.; Ercelebi, M. *J. Mater. Sci.* **2004**, *15*, 225−229.
(35) Ghosh, S.; Hoogland, S.; Sukhovatkin, V.; Levina, L.; Sargent, E. H. *Appl. Phys. Lett.* **2011**, *99*, 101102−101104.
(36) Singh, R.; Shewchun, J. *Appl. Phys. Lett.* **1978**, *33*, 601−603.